Applied Physics Letters

High performance WSe_2 p-MOSFET with intrinsic n-channel based on back-to-back p–n junctions

Cite as: Appl. Phys. Lett. **118**, 233101 (2021); https://doi.org/10.1063/5.0036343
Submitted: 04 November 2020 . Accepted: 25 May 2021 . Published Online: 07 June 2021

Xiaochi Liu, Yuchuan Pan, Junqiang Yang, Deshun Qu, Huamin Li, Won Jong Yoo, and Jian Sun

Applied Physics Letters ARTICLE scitation.org/journal/apl

High performance WSe_2 p-MOSFET with intrinsic n-channel based on back-to-back p–n junctions

Cite as: Appl. Phys. Lett. **118**, 233101 (2021); doi: 10.1063/5.0036343
Submitted: 4 November 2020 · Accepted: 25 May 2021 ·
Published Online: 7 June 2021

Xiaochi Liu,[1] Yuchuan Pan,[1] Junqiang Yang,[1] Deshun Qu,[2] Huamin Li,[3] Won Jong Yoo,[2,a)] and Jian Sun[1,a)]

AFFILIATIONS

[1]School of Physics and Electronics, Central South University, 932 South Lushan Road, Changsha 410083, China
[2]SKKU Advanced Institute of Nano-Technology (SAINT), Sungkyunkwan University, 2066 Seobu-ro, Jangan-gu, Suwon, Gyeonggi-do 16419, South Korea
[3]Department of Electrical Engineering, University at Buffalo, The State University of New York, Buffalo, New York 14260, USA

[a)]**Authors to whom correspondence should be addressed:** yoowj@skku.edu and jian.sun@csu.edu.cn

ABSTRACT

Most of the reported field effect transistors (FETs) in two-dimensional (2D) semiconducting transition metal dichalcogenides (TMDs) are based on the high power consumption Schottky FETs, in which the switching of current relies on the electrostatic modulation of the Schottky barrier at the metal–TMD contact interfaces. Even worse, they have been often mistakenly referred to as 2D metal-oxide-semiconductor field effect transistors (MOSFETs), which, however, have restricted design rules. Here, we demonstrate a two-dimensional p-MOSFET with an intrinsic n-type WSe_2 channel. This MOSFET consists of two back-to-back p–n junctions. With a hexagonal boron nitride van der Waals stacking mask, degenerate p-doping to WSe_2 from the oxidized surface can be selectively induced to the contact areas by controlled oxygen plasma, while maintaining the center of the channel intrinsic. Compared to Schottky FETs, outstanding device performances are realized, e.g., low field effect threshold, much reduced subthreshold swing, high on/off ratio exceeding 10^8, hole mobility as high as 191 $cm^2\ V^{-1}\ s^{-1}$, and hysteresis-free transfer characteristics.

The cornerstone of today's advanced complementary metal-oxide-semiconductor (CMOS) technology is the so-called metal-oxide-semiconductor field effect transistor (MOSFET), which is advantageous over other FET architectures because of its outstanding switching performance, such as low field effect threshold and low off-state leakage current. A proper MOSFET is constructed with two back-to-back p–n junctions. Its current switching relies on the formation of an inversion channel, where the minority carrier dominates the on-state transport. Its fabrication requires degenerately doping the native materials to the opposite polarity to form p–n junctions and to serve as contacts. For instance, the contact regions of a p-MOSFET should be degenerately doped to p^+ while keeping the intrinsic channel as n-type.

Two-dimensional (2D) semiconducting transition-metal dichalcogenides (TMDs) are of great interest for building next-generation electronics due to their uniform atomic thickness and unique electronic properties.[1–3] Particularly, their FETs provide a superior immunity to short channel effects, therefore attracting much attention. Realizing a MOSFET in 2D TMDs is of great importance. However, in the initial stage, controlled degenerate doping, especially the p-type doping, was technically challenging for 2D TMDs. Subsequently, the majority of the 2D FETs reported were Schottky transistors, in which the current switching relies on the modulation of a Schottky barrier at the metal–TMD contact interfaces.[4] In such Schottky transistors, large contact resistance is inevitable, leading to high power consumption. Hence, eventually research focus has been reorientated to reducing the contact resistance for TMDs. Various approaches, such as metal work function engineering[5,6] and chemical doping,[7,8] have been developed to reduce the Schottky barrier at the metal–TMD interface. Nevertheless, these strategies, which enhance the majority carrier transport, cause significantly shifted threshold voltage toward higher positive or negative gate voltages. The Schottky transistors show subthreshold swing much larger than 60 mV/dec at room temperature and ambipolar transfer characteristics even in an ideal device architecture. To realize 2D FETs with superior switching characteristics, a MOSFET based on p–n junctions is still the optimized option. Nevertheless, a 2D semiconductor-based MOSFET has rarely been demonstrated. Compared to the 2D Schottky transistor, its essential distinction has not been thoroughly discussed.

Recently, research found that transition metal oxides with a high work function, such as WO_x and MoO_x, are efficient p-type dopants to their relative TMDs.[9] Among different surface oxidation approaches, oxygen plasma treatment, which is compatible to the conventional semiconductor processing techniques, shows high potential as an effective p-type doping technique.[10–13] With Raman, photoluminescence, and x-ray photoelectron spectroscopic measurements, it has been confirmed that oxygen plasma can induce the selective oxidation on the topmost layer based on the layer-by-layer process.[13–15] By carefully controlling the plasma power and treatment durations, good tunability in doping concentration can be realized. Furthermore, we have also realized the spatial selective surface doping to TMD by using capping masks.[16] Technically speaking, we should, already, be prepared to realize the decent p-MOSFET in 2D TMDs.

In this Letter, we demonstrate a 2D p-MOSFET in WSe_2 with intrinsic n-type channel, which consists of two back-to-back p–n junctions. The degenerate p^+-doped contact regions are realized by the spatially controlled oxygen plasma doping with a van der Waals (vdW) capping mask. The switching characteristics of intrinsic WSe_2 Schottky FET, channel-doped WSe_2 Schottky FET, and WSe_2 MOSFET with degenerate contact doping are investigated and compared with each other. The WSe_2 MOSFET based on back-to-back p–n diodes is distinguished from those of the Schottky FETs with a steep turn on launched around 0 V gate voltage and much reduced subthreshold swing. High on/off ratio exceeding 10^8, large hole mobility of 191 $cm^2\ V^{-1}\ s^{-1}$, and transfer characteristics with negligible hysteresis are obtained in this p-MOSFET.

Fabrication starts by mechanically exfoliating few-layer WSe_2 on the heavily doped silicon substrate covered with 285 nm thermal SiO_2. WSe_2 flakes of ~10 nm-thick are selected under optical microscope by color and contrast, which later is verified by atomic force microscope. Metal contacts to WSe_2 are evaporated with palladium (Pd)/gold (Au) (20 nm/40 nm) stack using conventional nanofabrication techniques. Thin hexagonal boron nitride (h-BN) mask is mechanically exfoliated from its bulk crystal and dry-transferred onto the center of WSe_2 channel forming a vdW heterostructure.[17] Good alignment $<1\ \mu m$ can be guaranteed using a home-made mechanical manipulator.[18] Oxygen plasma treatment is carried out at room temperature in an inductively coupled plasma system equipped with a 13.56 MHz microwave source (Miniplasma-station, Plasmart) at constant oxygen flow of 30 sccm and pressure of 20 Pa. The lowest power to generate stable plasma at the pressure of 20 Pa in this system is 20 W. 1 W is the finest power increment allowed by this system. During the treatment, the power is not turned on to generate plasma until the pressure and flow rate are stabilized. Electrical measurements are performed in a vacuum probe-station at low pressure of ~0.1 Pa and various temperatures. To measure the FET performance of the WSe_2 devices, heavily doped silicon substrate acts as back gate with SiO_2 as dielectric layer.

First, we present the device performance of a typical Schottky FET made of pristine WSe_2 and with high work function Pd as contact. In Fig. 1(a), the ambipolar characteristic is observed in the measured transfer curve, known that the electron affinity of WSe_2 is 3.8 eV and the bandgap of few-layer WSe_2 is ~1.3 eV. Pd with the work function of 5.12 eV aligns to WSe_2 at its valence band edge as illustrated in Fig. 1(b), which ideally leads to a p-type characteristic. The conduction minimum point (CMP) appears at negative gate voltage

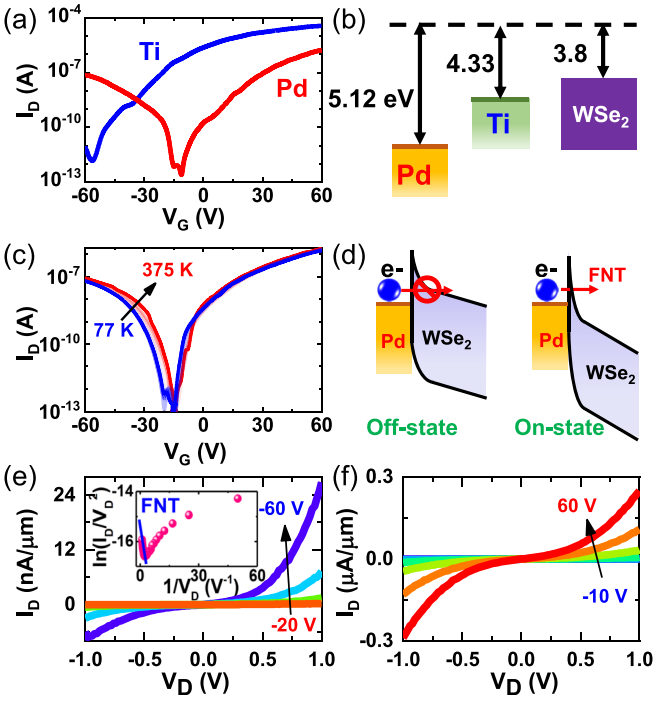

FIG. 1. (a) Transfer characteristics of WSe_2 FETs with Pd and Ti contacts. *t*: 8 nm, *l*: 2 μm, *w*: 3 μm. (b) Band alignment between WSe_2 and metals. The dashed line is the vacuum level. The numbers indicate the values of work function for metal and electron affinity energy for WSe_2. (c) Temperature dependence of the transfer characteristics. (d) Band diagrams showing the off-state and on-state governed by Fowler–Nordheim tunneling (FNT) at the contact interface. Output curves of (e) p-branch (f) and n-branch. Inset of (e): FNT fitting of the p-branch data at $V_G = -60$ V.

V_G. By changing the contacts into titanium (Ti) with a work function of 4.33 eV, CMP can be shifted significantly toward negative V_G in agreement with the previous report.[19] Hence, the observed ambipolar transfer characteristic is probably attributed to the weak Fermi level pining between Pd and WSe_2. Moreover, the negative CMP manifests pristine WSe_2 as an intrinsic n-type material. Temperature dependence of transfer curves can be used to explore the carrier transport mechanism for the pristine WSe_2 FET. Figure 1(c) shows the transfer curves measured at varied temperatures from 77 K to 375 K. The weak temperature dependence is noted, suggesting the dominance of Fowler–Nordheim tunneling (FNT) through a high Schottky barrier for both electron and hole.[20] Under this circumstance, tunneling current is switched on and off by tuning the barrier electrostatically by the gate as illustrated in Fig. 1(d). The existence of the high Schottky barrier is implied by the nonlinear and asymmetric output curves [Figs. 1(e) and 1(f)] and can be further verified by the good fit of FNT model to the p-branch output data ($V_G = -60$ V) at high bias V_D as shown in the inset of Fig. 1(e). Set aside the work function difference and pinning induced threshold voltage discrepancy between Pd and Ti contacted Schottky barrier FETs, ambipolar device characteristics, that is, electron transport for large positive gate voltages and hole transport for large negative gate voltages, are inevitable in those Schottky barrier FETs. This leads to high static power consumption of the device. Also considering the low hole current at ~10 nA/μm, even with high biases

of $V_G = -60$ and $V_D = 1$ V, this pristine WSe_2 Schottky FET is sub-optimal for real applications.

Next, the unipolar 2D Schottky p-FET is demonstrated by introducing p-type surface doping to WSe_2 with oxygen plasma. As-fabricated WSe_2 FET is treated by oxygen plasma at 20 W, that is the lowest power to introduce plasma. Plasma oxidizes the surface of WSe_2 into WO_x ($x < 3$)—an effective p-dopant to WSe_2—as illustrated in Fig. 2(a), and therefore, p-dopes the underlying WSe_2. In Fig. 2(b), temporal evaluation of transfer curves of plasma treated FET is plotted. Pristine FET is ambipolar with CMP at ~ -20 V. With longer treatment, CMP monotonically shifts to more positive V_G, acting as a solid evidence of induced p-doping. After 120 s treatment, a unipolar-like p-FET is obtained. Hole current gradually increases, as a result of reduced effective Schottky barrier.[21] It is worth to point out that the ambipolar transfer characteristics are still preserved with its CMP moving out of the measurement range. Quasi-linear and symmetric I–V output curves are measured in the device subjected to the 600-s-long treatment [Fig. 2(c)], which are frequently observed in Schottky transistors as a result of substantial tunneling via the Schottky barriers at the contacts.

Although inducing p-doping to WSe_2 benefits with enhanced hole transport and much improved contact condition, the increased off-state current and threshold voltage cause high power consumption issue. More importantly, plasma inevitably induces defects and charged disorders to the WSe_2 channel, resulting in the considerable hysteresis between the transfer curves measured in the forward and reverse V_G scans. In Fig. 2(d), transfer curves of the device after 600 s treatment are plotted in both forward and reverse scans of V_G, showing pronounced counterclockwise hysteresis. From these data, we are allowed to extract activation energy by fitting the temperature-dependent conductance G with thermal activation model, where $G \propto e^{-\left(\frac{E_a}{k_B T}\right)}$ with E_a and k_B being the activation energy and Boltzmann's constant, respectively.[22] The extracted E_a as a function of V_G is shown in the inset of Fig. 2(d), which is tuned from 12 meV at $V_G = 60$ V to 5.5 meV at $V_G = -60$ V. The extracted small activation energy is attributed to thermal emission of electrons from valence band to a shallow acceptor level, which reveals the formation of defect states near the valence band edge induced by the plasma treatment. Subsequently, serious scattering and associated suppressed hole mobility are inevitable.[23] Field effect mobility is extracted from transfer curve using Y-function method, which can effectively eliminate the impact of contact resistance. Y is defined as $\frac{I}{\sqrt{g_m}}$ with $g_m = dI_D/dV_G$ being the transconductance. I_D is drain current expressed as[24]

$$I_D = \left(\frac{\mu}{1 + \theta(V_G - V_T)}\right) C_{ox} \frac{w}{l} (V_G - V_T) V_D, \tag{1}$$

where C_{ox} is gate capacitance, l and w are the channel length and width, respectively, θ is a V_G dependent attenuation factor, and V_T is threshold voltage fitted from $Y - V_G$ curve. Mobility, therefore, is calculated by the expression

$$\mu = \left(\frac{Y}{V_G - V_T}\right)^2 \left(\frac{L}{C_{ox} W V_D}\right). \tag{2}$$

We calculate the mobility values as 19 and 24 and 30 $cm^2\ V^{-1}\ s^{-1}$ from Eq. (2) for the Schottky FET treated by 300, 420, and 600 s plasma, respectively, which are much lower than the previously reported value for pristine WSe_2.[25] Noted that as the strong inversion region is not reached in the Schottky FET with shorter plasma treatment, Y function model is not applicable to extract the mobility.

To build a MOSFET, degenerate p-doping is mandatory. We notice that doping strength is extremely sensitive to the plasma power and can be dramatically enhanced by increasing the power to 21 W. The transfer curves measured before and after the treatments of varied durations at 21 W are plotted in Fig. 3(a). Heavily p-doped characteristic starts to emerge even with a short treatment of 100 s. After 300 s, hole current density already reaches 50 $\mu A/\mu m$. It corresponds to an extremely high hole sheet density of $\sim 10.3 \times 10^{12}$ cm^{-2} [Fig. 3(b)], far exceeding the lower limit of degenerate doping for 2D TMDs.[26] Detail of the hole sheet density extraction is presented in the supplementary material. Such degenerately doped WSe_2 is almost metallic, with the current only modulated by 2.5 times within the applied V_G range. Considering the relatively high pressure of 20 Pa, lateral effect of the plasma also causes the oxidation and doping to the WSe_2 under metal contacts.[13] Hence, metal contacts can have the direct touch to degenerately doped WSe_2 near their edges as illustrated in Fig. 3(c), which highly suppresses Schottky barrier at the interface and improves the contact condition. Using a transmission line model (TLM) device [inset of Fig. 3(d)], contact resistance R_C and sheet resistance R_S for the degenerately doped WSe_2 are quantitatively evaluated.[27] Figure S1 in supplementary material plots the output curves measured at different channels in the TLM device. The extracted R_C and R_S in the WSe_2 treated by 300 s are plotted as a function of V_G in Fig. 3(d). The relatively low R_C and R_S of 5.6 $k\Omega \cdot \mu m$ and 6 $k\Omega/\square$ are observed at zero gate. R_C can be further reduced from 7.4 to 3.6 $k\Omega \cdot \mu m$ by V_G modulation, while R_S can be lowered to 2 $k\Omega/\square$. For comparison, a four orders of magnitude higher R_C of 100 $M\Omega \cdot \mu m$ is estimated for the contact-dominated pristine device, where the total resistance of the device is mostly contributed from the two contacts.

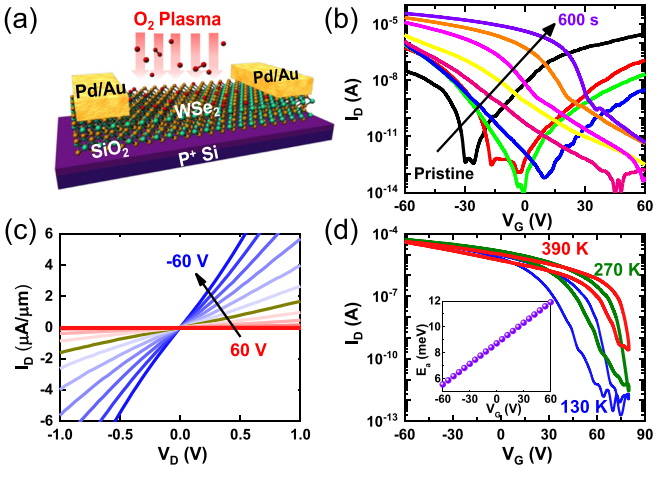

FIG. 2. (a) Illustration showing oxidation on the surface of WSe_2 FET during oxygen plasma treatment. (b) Transfer curves of a WSe_2 FET measured after oxygen plasma of 0, 5, 20, 60, 120, 180, 300, 420, and 600 s with fixed power of 20 W. *t*: 9 nm, *w*: 2 μm, *l*: 2 μm, $V_D = 1$ V. (c) Output curves of the WSe_2 FET after 600 s plasma at various V_G. (d) Transfer curves showing counterclockwise hysteresis loops in forward and reserve V_G scans measured at varied temperatures in the 600 s treated FET. Inset: extracted activation energy as a function of V_G.

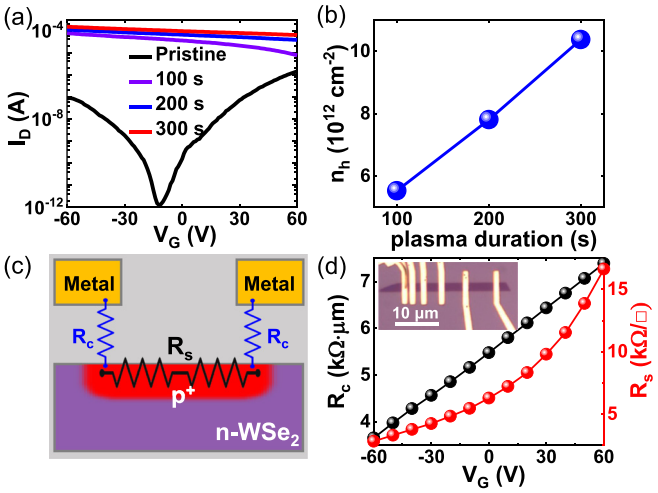

FIG. 3. (a) Evolution of transfer curves of WSe_2 FET after various plasma treatment durations with power of 21 W. *t*: 9 nm, *w*: 1.5 μm, *l*: 2 μm, $V_D = 1$ V. (b) Sheet hole density as a function of treatment durations. (c) Schematic of metal contacted degenerately p-doped WSe_2. R_C and R_S represent the contact resistance and sheet resistance, respectively. (d) R_C and R_S as a function of V_G of WSe_2 FET subjected to a 300 s plasma. Inset: optical microscopy image of a TLM device. *t*: 8 nm, *w*: 1.5 μm.

Technically, using a capping mask to protect part of the WSe_2 from oxygen plasma, we can spatially control the plasma doping at the exposed area.[16] Hence, a lateral WSe_2 p–n junction, which is a prerequisite for fabricating WSe_2 p-MOSFET, can be realized. Here, h-BN flake is utilized as the capping mask. A h-BN flake with high quality crystalline can be mechanically exfoliated from a single crystal bulk, and it can be transferred onto WSe_2 channel with pretty good alignment precision using the vdW stacking technique. In this work, the relatively thick h-BN flakes are used as mask since a large flake is easier to be exfoliated and found. In fact, we note a negligible etching effect on h-BN by the weak oxygen plasma. It suggests that thinner h-BN flake with atomic thickness can act as an efficient doping mask. Moreover, thanks to the inert property of h-BN and clean interface of the vdW heterostructure, the impact brought by the capping h-BN mask to the underlying WSe_2 is nearly negligible. In Fig. 4(a), we plot the transfer characteristic of a WSe_2 FET before and after transferring the h-BN mask. No shift of CMP is noticed, indicating negligible doping induced by h-BN mask. On contrary, the electron branch is improved with the enhanced mobility, which is probably ascribed to reduced scatterings from surrounding impurities due to h-BN passivation. The WSe_2 p–n junction is, then, simply fabricated by transferring thin h-BN to cover half of the WSe_2 channel. The optical microscopy image of the fabricated device is shown in the inset of Fig. 4(b). After inducing p-doping to the exposed area with oxygen plasma, a p–n junction is, therefore, formed. It can be verified by the typical p–n junction output curve, which exhibits a large rectifying ratio up to 10^5 [Fig. 4(b)].

In the end, we demonstrate WSe_2 p-MOSFET with degenerately doped p$^+$ contacts and an intrinsic n-type channel. Plasma-induced degenerate p-doping is spatially controlled at the contact areas with the h-BN vdW capping mask [Fig. 5(a)]. Figure 5(b) shows a WSe_2 device with a h-BN vdW mask capped on the center of the channel.

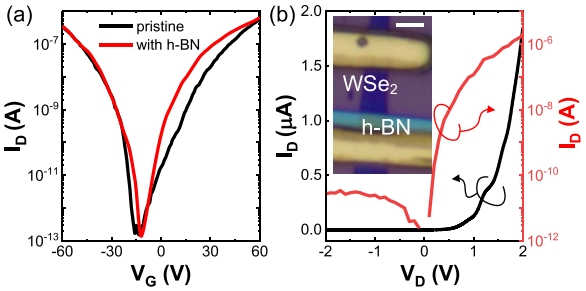

FIG. 4. (a) Transfer curves of a WSe_2 FET with and without vdW h-BN mask. (b) The *I*–*V* characteristic of a WSe_2 p–n junction device made by spatially selected oxygen plasma doping. $V_G = 60$ V. The current I_D is plotted in both linear and logarithm scale. Inset: optical microscope image of the p–n junction device. A h-BN mask (light blue, *t*: 20 nm) is capped on half of the WSe_2 (dark purple) channel. Scale bar: 2 μm.

After oxygen plasma treatment, two back-to-back p–n junctions are formed between p$^+$ contacts and intrinsic n-channel. Theoretically, switching mechanism changes to that illustrated in Fig. 5(c). At off-state, diffusion of the majority charge carriers, i.e., holes in contacts and electrons in channel, is blocked by the built-in barrier in p–n junctions. Off-state leakage current originated from minority carrier drift is expected to be low. At on-state, thanks to the low thickness of WSe_2 channel, back gate modulation is efficient to completely deplete electrons and leads to an inversion p-channel. Subsequently, holes can be injected from contacts to the channel. Figure 5(d) plots the temporal evolution of transfer curves of the MOSFET subjected to the 21 W

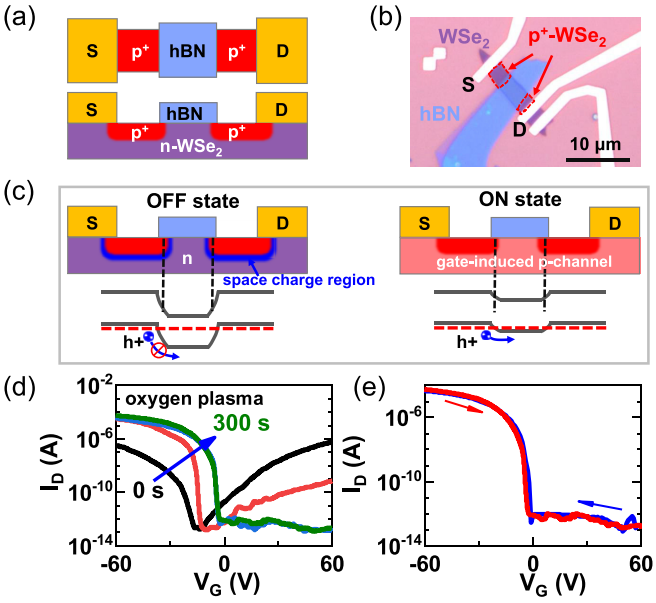

FIG. 5. (a) Schematics of top- and side-view of WSe_2 p-MOSFET with p$^+$ doped contacts and pristine n-channel. (b) Optical microscopy image of WSe_2 p-MOSFET. *t*: 10 nm, *w*: 3 μm, h-BN thickness: 12 nm, capped channel length: 3.5 μm. (c)Schematics and band diagrams of p-MOSFET at off and on states. (d) Transfer curves of WSe_2 FET with h-BN mask after varied plasma treatment durations. $V_D = 1$ V. (e)Transfer curves of p-MOSFET (300 s treatment) in forward and reserve V_G scans. Scan directions are indicated by the arrows.

oxygen plasma for varied durations. After 100 s, ambipolar FET characteristic changes to the hole dominated one. Hole current is enhanced by two orders, while the electron branch is lowered dramatically by three orders. After 300 s plasma, degenerate p^+-doping results in sufficient high built-in barriers in p–n junctions to fully block electron transport; the off-state current is, therefore, maintained consistently low even at a large positive V_G. Transfer characteristic of a real unipolar enhancement p-MOSFET is obtained with a sharp transition from OFF to ON state at $V_G \sim 0$. A large on/off ratio exceeding $\sim 10^8$ and high on-current of 6×10^{-5} A are measured. Knowing the channel width of 3 μm, current density is as high as 20 μA/μm. In addition, compared to the plasma doped Schottky p-FET, the channel of MOSFET is protected by the flat and inert h-BN mask from plasma-induced defects, therefore maintaining its intrinsic properties.[28] Subsequently, negligible hysteresis is measured in the MOSFET as plotted in Fig. 5(e), implying the neglected charged disorders induced in protected WSe_2 channel. As a result, a considerable hole mobility as high as 191 $cm^2\ V^{-1}\ s^{-1}$ is extracted for the WSe_2 MOSFET by fitting the Y-function model to the measured transfer curve. Note that the exposed areas are degenerately doped and, therefore, transit into contacts. Hence, the actual channel length for the extraction is the capped length underneath the h-BN mask. Here, to highlight the significance of the h-BN mask, we also fabricate a MOSFET using PMMA as capping mask. A weak hysteresis is identified in the transfer curves while a lower hole mobility of 86 $cm^2\ V^{-1}\ s^{-1}$ is extracted, as PMMA offers a poorer interface quality than h-BN (Fig. S2 in supplementary material). Nevertheless, the extracted mobility is much higher than that of the Schottky transistor since the channel of MOSFET is essentially protected from the plasma-induced defects. A subthreshold swing (SS) of 320 mV/dec is extracted, attributed to the pure thermionic carrier injection process with negligible contact resistance. Considering the relatively thick SiO_2 dielectric of 300 nm, this value indeed is impressively low, while the typical SS reported in the 2D Schottky FETs ranges from >0.5 V/dec to a few V/dec, as a result of the mixed carrier injection mechanisms from both thermionic emission and tunneling at the contacts.[29–31] Using high-κ dielectrics to reduce the effective oxide thickness, the SS of the WSe_2 p-MOSFET is expected to be dramatically reduced further.

In summary, we demonstrate a p-MOSFET in 2D WSe_2 with degenerately p-doped contacts and an intrinsic n-channel. Spatially controlled p-doping is induced by oxygen plasma with a h-BN vdW capping mask. The MOSFET device can be distinguished from Schottky FETs by a steep turn-on launched around 0 V gate voltage and much reduced subthreshold swing, therefore significantly reducing the power consumption for operation. Moreover, the p-MOSFET defeats a conventional p-doped Schottky FET with other outstanding performances, such as large on/off ratio of $>10^8$, negligible hysteresis, and hole mobility as high as 191 $cm^2\ V^{-1}\ s^{-1}$. This spatially selected plasma doping technique can be utilized for realizing various electronic devices with 2D TMDs, such as p–n diodes and tunnel FETs. We envisage that the 2D MOSFET can be realized by using other doping methods as long as they can introduce stable degenerate doping to 2D semiconductors.

See the supplementary material for the details of the hole sheet density extraction, output curves measured in the TLM device, and the transfer curves measured in the MOSFET fabricated with a PMMA mask.

This work was partially supported by the National Natural Science Foundation of China (Grant No. 11804397) and Hunan High-level Talent Program (Grant No. 2019RS1006). This work was also partially supported by the Global Research Laboratory (GRL) Program (No. 2016K1A1A2912707) and the Global Frontier R&D Program (No. 2013M3A6B1078873), both funded by the Ministry of Science, ICT & Future Planning via the National Research Foundation of Korea (NRF).

DATA AVAILABILITY

The data that support the findings of this study are available from the corresponding author upon reasonable request.

REFERENCES

[1]V. Podzorov, M. E. Gershenson, C. Kloc, R. Zeis, and E. Bucher, Appl. Phys. Lett. **84**, 3301 (2004).
[2]S. Manzeli, D. Ovchinnikov, D. Pasquier, O. V. Yazyev, and A. Kis, Nat. Rev. Mater. **2**, 17033 (2017).
[3]Q. H. Wang, K. Kalantar-Zadeh, A. Kis, J. N. Coleman, and M. S. Strano, Nat. Nanotechnol. **7**, 699 (2012).
[4]H. Liu, M. Si, Y. Deng, A. T. Neal, Y. Du, S. Najmaei, P. M. Ajayan, J. Lou, and P. D. Ye, ACS Nano **8**, 1031 (2014).
[5]W. Liu, J. Kang, D. Sarkar, Y. Khatami, D. Jena, and K. Banerjee, Nano Lett. **13**, 1983 (2013).
[6]S. Das and J. Appenzeller, Appl. Phys. Lett. **103**, 103501 (2013).
[7]H. Fang, S. Chuang, T. C. Chang, K. Takei, T. Takahashi, and A. Javey, Nano Lett. **12**, 3788 (2012).
[8]H. Fang, M. Tosun, G. Seol, T. C. Chang, K. Takei, J. Guo, and A. Javey, Nano Lett. **13**, 1991 (2013).
[9]M. Yamamoto, S. Dutta, S. Aikawa, S. Nakaharai, K. Wakabayashi, M. S. Fuhrer, K. Ueno, and K. Tsukagoshi, Nano Lett. **15**, 2067 (2015).
[10]I. Moon, S. Lee, M. Lee, C. Kim, D. Seol, Y. Kim, K. H. Kim, G. Y. Yeom, J. T. Teherani, J. Hone, and W. J. Yoo, Nanoscale **11**, 17368 (2019).
[11]P. R. Pudasaini, A. Oyedele, C. Zhang, M. G. Stanford, N. Cross, A. T. Wong, A. N. Hoffman, K. Xiao, G. Duscher, D. G. Mandrus, T. Z. Ward, and P. D. Rack, Nano Res. **11**, 722 (2018).
[12]A. N. Hoffman, M. G. Stanford, M. G. Sales, C. Zhang, I. N. Ivanov, S. J. McDonnell, D. G. Mandrus, and P. D. Rack, 2D Mater. **6**, 045024 (2019).
[13]X. Liu, D. Qu, Y. Yuan, J. Sun, and W. J. Yoo, ACS Appl. Mater. Interfaces **12**, 26586 (2020).
[14]H. Zhu, X. Qin, L. Cheng, A. Azcatl, J. Kim, and R. M. Wallace, ACS Appl. Mater. Interfaces **8**, 19119 (2016).
[15]Z. Li, S. Yang, R. Dhall, E. Kosmowska, H. Shi, I. Chatzakis, and S. B. Cronin, ACS Nano **10**, 6836 (2016).
[16]X. Liu, Y.-H. Yuan, D. Qu, and J. Sun, Phys. Status Solidi RRL **13**, 1900208 (2019).
[17]A. Castellanos-Gomez, M. Buscema, R. Molenaar, V. Singh, L. Janssen, H. S. J. van der Zant, and G. A. Steele, 2D Mater. **1**, 011002 (2014).
[18]J. Sun, R. S. Deacon, R. Wang, J. Yao, C. M. Lieber, and K. Ishibashi, Nano Lett. **18**, 6144 (2018).
[19]P. R. Pudasaini, M. G. Stanford, A. Oyedele, A. T. Wong, A. N. Hoffman, D. P. Briggs, K. Xiao, D. G. Mandrus, T. Z. Ward, and P. D. Rack, Nanotechnology **28**, 475202 (2017).
[20]X. Liu, Y. Yuan, Z. Wang, R. S. Deacon, W. J. Yoo, J. Sun, and K. Ishibashi, Phys. Rev. Appl. **13**, 044056 (2020).
[21]F. Giannazzo, G. Fisichella, G. Greco, S. D. Franco, I. Deretzis, A. La Magna, C. Bongiorno, G. Nicotra, C. Spinella, M. Scopelliti, B. Pignataro, S. Agnello, and F. Roccaforte, ACS Appl. Mater. Interfaces **9**, 23164 (2017).
[22]B. Radisavljevic and A. Kis, Nat. Mater. **12**, 9 (2013).
[23]S. I. Khondaker and M. R. Islam, J. Phys. Chem. C **120**, 13801 (2016).
[24]H.-Y. Chang, W. Zhu, and D. Akinwande, Appl. Phys. Lett. **104**, 113504 (2014).
[25]H. C. P. Movva, A. Rai, S. Kang, K. Kim, B. Fallahazad, T. Taniguchi, K. Watanabe, E. Tutuc, and S. K. Banerjee, ACS Nano **9**, 10402 (2015).

[26]J. Suh, T.-E. Park, D.-Y. Lin, D. Fu, J. Park, H. J. Jung, Y. Chen, C. Ko, C. Jang, Y. Sun, R. Sinclair, J. Chang, S. Tongay, and J. Wu, Nano Lett. **14**, 6976 (2014).
[27]R. Kappera, D. Voiry, S. E. Yalcin, B. Branch, G. Gupta, A. D. Mohite, and M. Chhowalla, Nat. Mater. **13**, 1128 (2014).
[28]A. K. Geim and I. V. Grigorieva, Nature **499**, 419 (2013).
[29]H.-J. Chuang, X. Tan, N. J. Ghimire, M. M. Perera, B. Chamlagain, M. M.-C. Cheng, J. Yan, D. Mandrus, D. Tománek, and Z. Zhou, Nano Lett. **14**, 3594 (2014).
[30]H.-J. Chuang, B. Chamlagain, M. Koehler, M. M. Perera, J. Yan, D. Mandrus, D. Tománek, and Z. Zhou, Nano Lett. **16**, 1896 (2016).
[31]C. Zhou, Y. Zhao, S. Raju, Y. Wang, Z. Lin, M. Chan, and Y. Chai, Adv. Funct. Mater **26**, 4223 (2016).